OPEN ACCESS Freely available online

Journal of Geology & Geophysics

Research Article

# Integrating 3D Seismic and Wireline Log Data for Optimum Hydrocarbon Exploration in the "USOR" Field, Onshore Niger Delta

**Unyime Ezekiel Ukpong[1*], Anthony Aniekan Akpan-Usese[2], Samuel Izama Ugar[1], Chiedozie Vincent Ekowu[1]**

*[1]Department of Geology, University of Calabar, Calabar, Nigeria; [2]Department of Atomic Energy, University of Calabar, Calabar, Nigeria*

## ABSTRACT

In this work, 3D seismic data and wireline logs have been integrated to carry-out the optimum hydrocarbon exploration in order to delineate and assess the viability of the available petroleum prospects for proper planning of exploitation programmes in the "USOR" field. The field, which covers an area of 178 km$^2$, is located onshore, on the coastal swamp depobelt of Niger delta. The standard method of identifying reservoirs and correlation based on log pattern, petrophysical analysis of the reservoirs, generation of synthetic seismograms, seismic-to-well tie and delineation of reservoir tops and bases as seismic horizons on seismic volume, fault mapping, generation of time- and depth-structure maps from the mapped horizons, delineation of prospects, modeling of reservoir petrophysical properties and volumetric analysis were employed. Three vertically stacked reservoirs (UR1 to UR3) were identified. Nine growth faults (F1 to F9) were mapped from which faults model have been generated. Time and depth-structure maps were generated from the mapped horizons of reservoir tops where three already drilled proven reserves and four new prospect areas (UR1(A), UR2(A), UR3(A) and UR2(B and C) and UR3(B and C), respectively) have been identified based on structural closure aided by maximum amplitude and average energy seismic volume attributes. The three reservoirs were modelled for its petrophysical properties and have been shown to be good to very good. Volumetric analysis, where both the deterministic and probabilistic (using Monte Carlo simulation method) approaches, of the identified proven reserve and prospects gave (unrisked) volumes of Gas Initially in Place (GIIP) of 570 MCF for deterministic and 1269.54 (P10), 828.17 (P50) and 344.22 (P90) MCF for probabilistic assessment. The Stock-Tank Oil Initially in Place (STOIIP) range from 71 to 541 MMSTB for the deterministic and 116 (P90) to 1260.09 (P10) for the probabilistic approach.

**Keywords:** 3D seismic; Wireline log; Seismic attribute; Reservoir model; Volumetric

## INTRODUCTION

Though there is challenging demand for alternative energy, global demand for oil and gas is still on the high side. This necessitate the need for more discoveries of hydrocarbon bearing zones. To achieve this, meticulously evaluating the potential of specific reservoirs bearing zones within geologically complex basin is required through rigorous and integrated approach. Hence, the proper and careful unification of exploration data set is an indispensable tool for the ultimate goal of adequately discovering economical accumulations of hydrocarbon thousands of meters beneath the earth's surface.

Hydrocarbon bearing zones can be delineated by quantitatively and precisely describing reservoir architectures and its properties using well logs, seismic and geological information. In the majority of reservoir development projects, the description of the reservoir is achieved through integrating well information and seismic data. The knowledge of reservoir dimension is an

**Correspondence to:** Unyime Ezekiel Ukpong, Department of Geology, University of Calabar, Calabar, Nigeria; E-mail: uy_ukpong@yahoo.com

**Received:** 14-Oct-2024, Manuscript No. JGG-24-34598; **Editor assigned:** 17-Oct-2024, PreQC No. JGG-24-34598 (PQ); **Reviewed:** 31-Oct-2024, QC No. JGG-24-34598; **Revised:** 16-Oct-2025, Manuscript No. JGG-24-34598 (R); **Published:** 23-Oct-2025, DOI: 10.35841/2381-8719.25.14.1247

**Citation:** Ukpong UE, Usese AAA, Ugar SI, Ekowu CV (2025) Integrating 3D Seismic and Wireline Log Data for Optimum Hydrocarbon Exploration in the "USOR" Field, Onshore Niger Delta. J Geol Geophy. 14:1247.

important factor in quantifying producible hydrocarbon reservoir. These parameters are important because they serve as veritable inputs for reservoir volumetric analysis. Exploration of enhanced data collection and analysis techniques has led to more accurate and comprehensive models of the subsurface, leading to a more enlightened and successful investment resolution. The integration of datasets helps in precise reservoir characterization, improved prediction accuracy, more efficient production planning, reduced environment risk, discovering of new economical fields, evaluating unconventional reservoirs, optimizing field development, etc.

The Niger Delta ranks amongst the 12$^{th}$ largest oil province in the world and the 2$^{nd}$ in Africa (after Angola). However, with this bequest and increasing demand for energy, there is still need for infill wells and discovering of new prospect areas. As a consequence, to this, more refined and detailed techniques are subsequently being employed, of which careful integration of data sets play a major role.

This study seeks to integrate the available data sets for the optimum exploration and subsequent exploitation of hydrocarbon in the "UsSOR" field, in the onshore part of Niger delta.

The "USOR" field is located onshore, on the coastal swamp Depobelt of the Niger delta basin (Figure 1). The basin is one of the large arcuate Tertiary regressive deltaic sequences in the world situated in the continental margin of the Gulf of Guinea in Equatorial West Africa between longitude 3°-8° E and latitude 4°-7° N. It owes it origin and present day framework to the result of rifting episodes that separated Africa from South America and the subsequent opening of the south Atlantic, which started in the Late Jurassic and persisted to the middle cretaceous. The subsurface tripartite stratigraphy of the delta consists of a continental shallow marine massive sand sequence-Benin Formation, coastal marine sequence of alternating sands and shales the Agbada formation and basal marine shale unit Akata formation, with the shales of the Agbada and Akata formation being the source rocks while the Eocene to Pliocene sands of the Agbada Formation form the main reservoirs. Traps are usually, faulted rollover anticlines associated with growth faults produced during varying degrees of both syn and post-depositional deformation with gravity tectonism as the primary deformation process. Stratigraphic Traps related to paleochannel fills, regional sand pinch-out and truncations also occur [1-3].

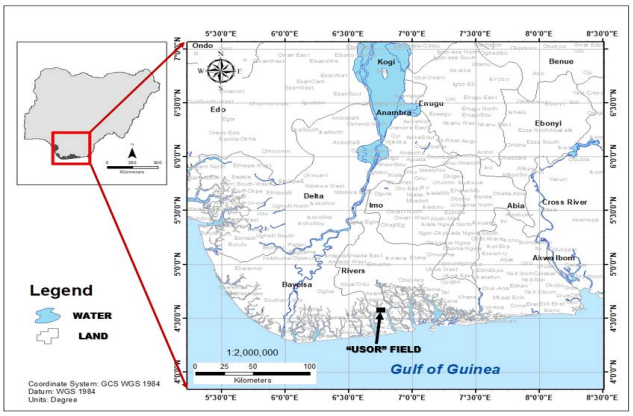


**Figure 1:** Map of Niger delta, showing the location of the "USOR" field.

# MATERIALS AND METHODS

## Materials

Materials available for this study include; (i) Suites of wireline logs from 6 wells (ii) A rectangular grid of 3D PSTM data which covers an area of 178 km$^2$ with 401 in-lines trending North-South and spaced 25 m apart and 221 crosslines trending east-west and equally spaced 25 m apart (Figure 2). The data, which extends up to 6 seconds (TWT) with variable density display, is provided in SEG-Y bricked format. Also available are checkshot data from the six wells.

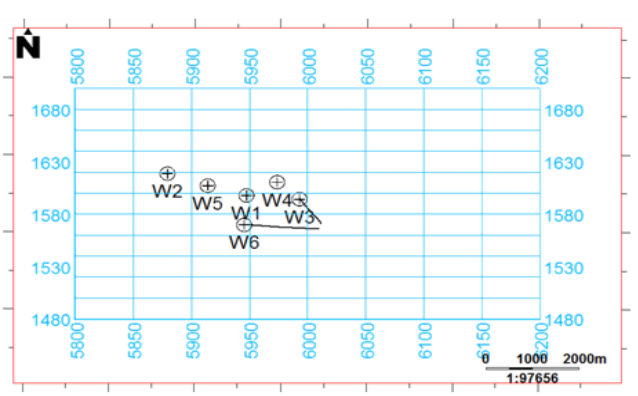


**Figure 2:** Base map of "USOR" field, showing the locations of wells (w), the representative North-South oriented inline and east-west oriented crosslines.

## Method

The workflow used in this study is presented in Figure 3.

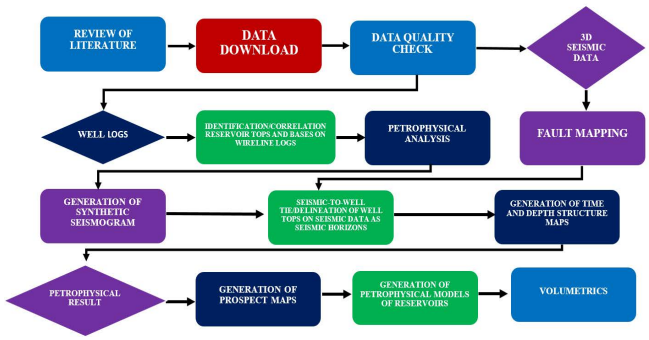


**Figure 3:** Workflow chart.

**Identification, correlation and petro physical analysis of reservoirs:** The equations which were inputted into the petrel software, were used to calculate and generate petro physical logs. These logs (total and effective porosities, permeability, volume of shale, facies, water and hydrocarbon saturation) in combination with gamma-ray, Spontaneous Potential (SP), sonic (DT) resistivity and density-neutron combination logs were used identify three reservoir intervals (UR1 to UR3) in the wells and correlated across the field (Figures 4 and 5). The types of fluids (water and hydrocarbon) filling the pore spaces were also identified using resistivity, neutron and density combination, water and hydrocarbon saturation logs. The contact between these two fluids (Oil and Water Contact, OWC) were also identified in all the six wells. No visible Gas-Oil Contact (GOC) could be inferred from the logs so no GOC was identified.

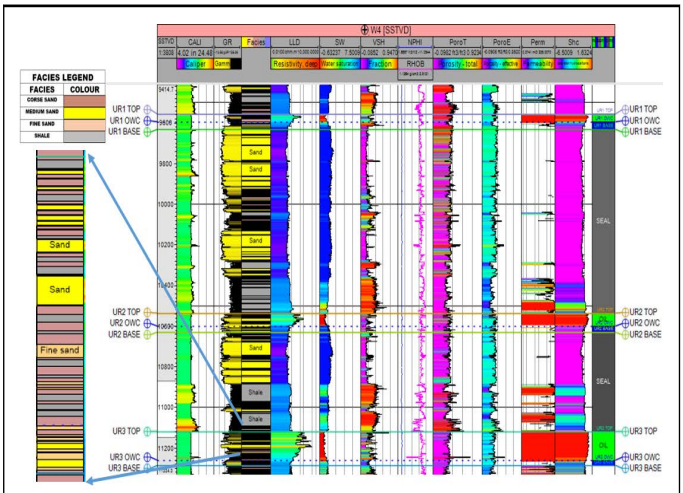


**Figure 4:** Well (4) section showing the caliper (CALI), Gamma Ray (GR), facies, deep resistivity (LLD), Water Saturation (SW), Volume of shale (Vsh), density (RHOB)-neutron (NPHI) combination, total and effective porosities, permeability, hydrocarbon saturation (Sh), fluid zones, reservoir (UR) tops and bases and Oil-Water Contacts (OWC). The enlarged part of the facies log indicate the different colors of the available facies. The black color is due to the compression of the scale.

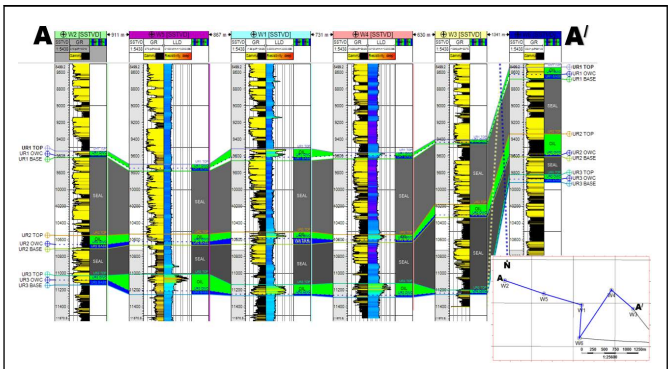


**Figure 5:** Well sections showing the correlation reservoir (UR) tops and bases across the six wells along line A-A/(blue line on inset basemap.

**Generation of synthetic seismograms:** Check shots from the six wells were used to generate the synthetic seismogram (Figure 6) for each of the wells. Reflectivity coefficient was calculated from changes in acoustic impedance which was then convolved with a zero phase Ricker wavelet of 25 Hz to generate the synthetic. An average bulk time shift of 4 ms (TWT) was applied to achieve a good tie with the seismic [4,5].

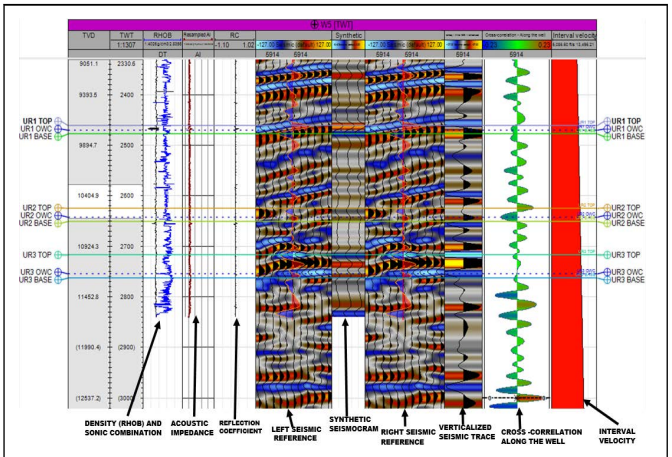


**Figure 6:** Well (5) section showing the generated synthetic seismogram, reservoir (UR) tops and bases and Oil-Water Contacts (OWC).

**Fault mapping:** Identification of faults on the seismic volume was based on vertical displacement and reflection discontinuity at faults planes. Also, some seismic volume attributes (structural smoothing and variance edge) (Figure 7) were also used to further enhance the visibility of these faults. The faults were then traced iteratively, at increments of 5 lines, on the inline and crossline directions. Faults model were generated from faults sticks for better understanding of the structural geometry of the field. Nine (9) major growth faults (F1 to F9) (Figure 8) were identified in the study area, each trending and dipping in various directions.

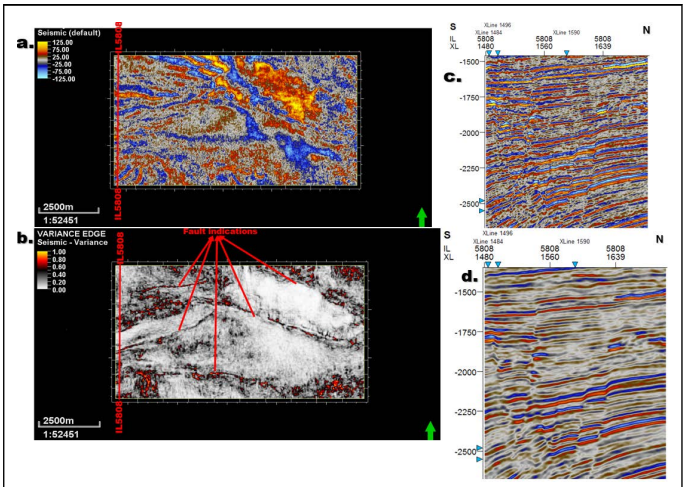


**Figure 7:** Time slice sections at -2552 ms (TWT) of (a) original seismic and (b) variance edge attribute (for better visualization of the faults) and inline (IL) sections 1508 of (c) original seismic and (d) structural smoothing, showing the fault indications clearly.

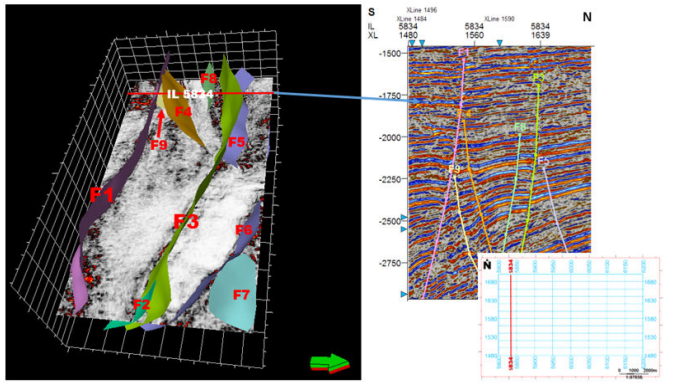


**Figure 8:** Time slice section (-2480 ms TWT) of variance edge attribute showing the faults model and inline section 5834 of the original seismic showing the intersected faults (F1, F3, F4, F5, F8 and F9).

**Seismic-to-well tie/delineation of reservoir tops and bases on seismic volume:** The generated synthetic seismograms were used to tie the wells to the seismic and the reservoir tops and bases traced on the seismic volume as seismic horizons both in the inline and crosslines directions (Figure 9). six horizons, displaced by growth faults common throughout the field area were mapped [6].

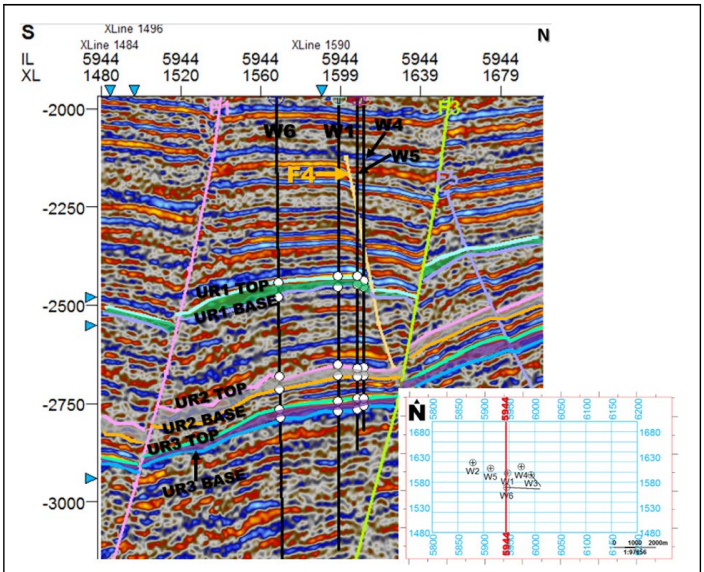


**Figure 9:** Inline section, 5944, showing wells (W) I, 4, 5 and 6, reservoir (UR) tops and bases and intersected fault (FI, F3, F4 and F5).

**Generation of time and depth structure maps:** The faults polygons, produced from the identified faults, were posted on the reservoir top horizons from where time-structure maps were generated. These time-structure maps were then converted to depth-structure maps, using a second order polynomial function derived from the Time-Depth Relationship (TDR) obtained from the check shot data (Figures 10-12).

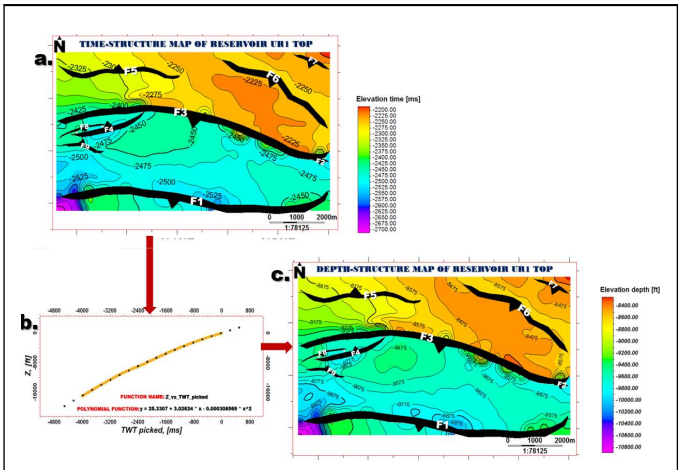


**Figure 10:** (a) Time-structure map of reservoir UR1 top, (b) time-depth relationship (TDR) plot, obtained from the checkshot in well 5 and the polynomial function used to convert the time to depth map and (c) depth structure map of reservoir UR1 top. F: Faults. Black triangle on the time and depth maps point towards the dip direction of faults. Contour interval on time and depth structure maps are 25 ms and 100 m (TWT), respectively.

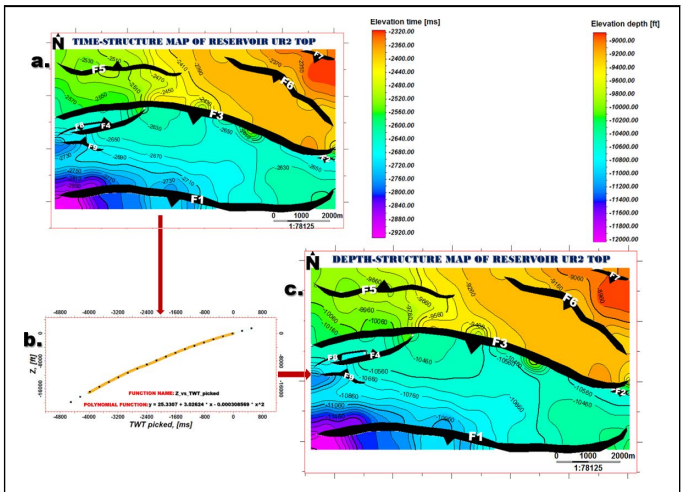


**Figure 11:** (a) Time-structure map of reservoir UR2 top, (b) Time-Depth Relationship (TDR) plot, obtained from the check shot in well 5 and the polynomial function used to convert the time to depth map and (c) depth-structure map of reservoir UR2 top. F – Faults. Black triangle on the time and depth maps point towards the dip direction of faults. Contour interval on time-and depth-structure maps are 20 ms and 100 m (TWT), respectively.

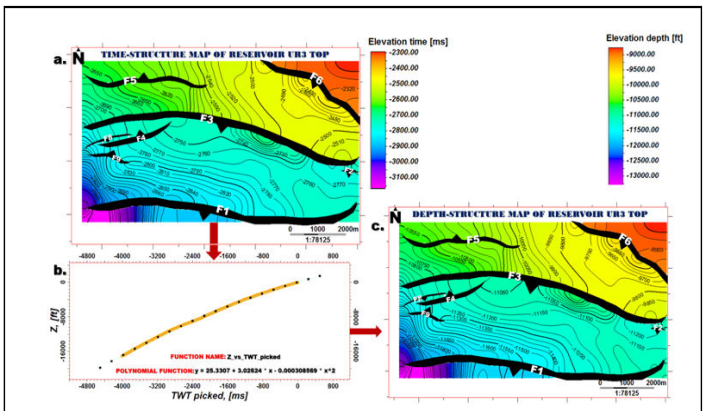


**Figure 12:** (a) Time-structure map of reservoir UR3 top, (b) Time-Depth Relationship (TDR) plot, obtained from the check shot in well 5 and the polynomial function used to convert the time to depth map and (c) depth-structure map of reservoir UR3 top. F: Faults. Black triangle on the time and depth maps point towards the dip direction of faults. Contour interval on time-and depth-structure maps are 10 ms and 50 m (TWT), respectively.

# RESULTS AND DISCUSSION

## Petro physical results

The physical (reservoir tops and bases, thicknesses, fluid contacts) and petro physical (volume of shale, total and effective porosities, permeabilities, water and hydrocarbon saturation) parameters were calculated to characterize the three (3) hydrocarbon reservoir units (reservoirs UR1 to U3R) across the seven (6) wells. The three Miocene, vertically stacked reservoirs (UR1 to UR3), exhibit fair to good physical and petro physical properties which makes them favorable to hold considerable amount of hydrocarbon for economic considerations [7-10].

## Prospect identification

Three (3) already drilled proven reserves (UR1(A), UR2(A) and UR3(A)) and four (4) new prospect areas (UR2(B and C) and UR3(B and C)) were identified based on faults and contour closures aided by the application of some seismic volume attribute (maximum amplitude and average energy) on the depth structure maps of the reservoir tops (Figures 13-15). Areas with high amplitude (suggested to be due to hydrocarbon accumulation) with respect to other parts of the map, aided by structural closures, were interpreted to be prospect areas. The four newly identified prospect areas and the three already proven reserves are located on the footwall side and on subtle rollover anticlinal structure at the hanging wall side of F5, F6 and F3, respectively. This conforms with the style of trapping (faulted rollover anticlines) common in the Tertiary Niger Delta basin as reported by many authors such as Evamy et al. UR1(A) contains gas cap, inferred from the anomalously high amplitude and a clear GOC could be seen. However, whereas other prospects also show anomalously high amplitude that may be attributed to gas presence, there is no clear GOC, both on the map and the wireline logs.

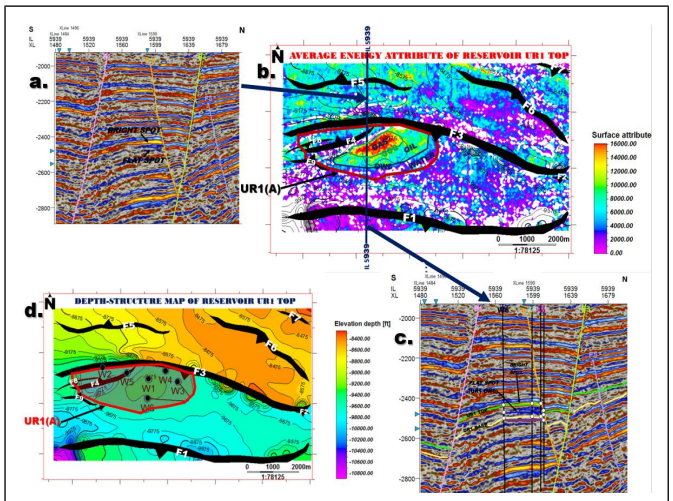


**Figure 13:** (a) inline (IL 5939), showing the Direct Hydrocarbon Indicators (DHI), bright and subtle flat spot and (b) average energy attribute of reservoir UR1 top showing the proven reserve, UR1(A) and the highlighted gas cap and Oil-Water Contact (OWC) which corresponds to the bright and flat spots, respectively on IL 5939. (c) Interpreted inline section 5939 showing the previously explained DHIs and UR1 top and base.(d) The already proven reserve which has been drilled by wells (W1-W6), was delineated based on seismic attribute on fault and contour closure on a subtle rollover anticlinal structure at the hanging wall side of F3.

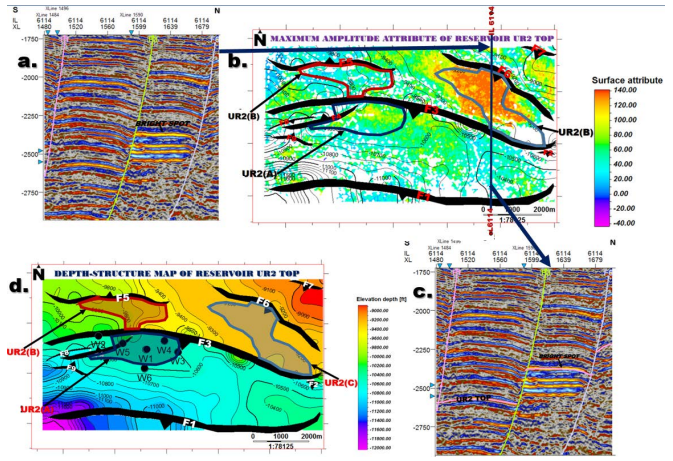


**Figure 14:** (a) inline (IL 6114), showing the direct hydrocarbon indicator (DHI) and (b) maximum amplitude attribute of reservoir UR2 top showing the proven reserve, UR2(A) and the newly identified prospect areas (UR2(B) and UR2C)) and the highlighted high amplitude due to hydrocarbon effect. (c) Interpreted inline section 6114 showing reservoir UR2 top and the anomalously high amplitude corresponding to prospect UR2(c). (d) The already proven reserve which has been drilled by wells (W1, W4 and W5) and the newly identified prospect areas, were delineated based on seismic attribute on fault and contour closure on a subtle rollover anticlinal structure at the hanging wall side of F3, F5 and F6, respectively.

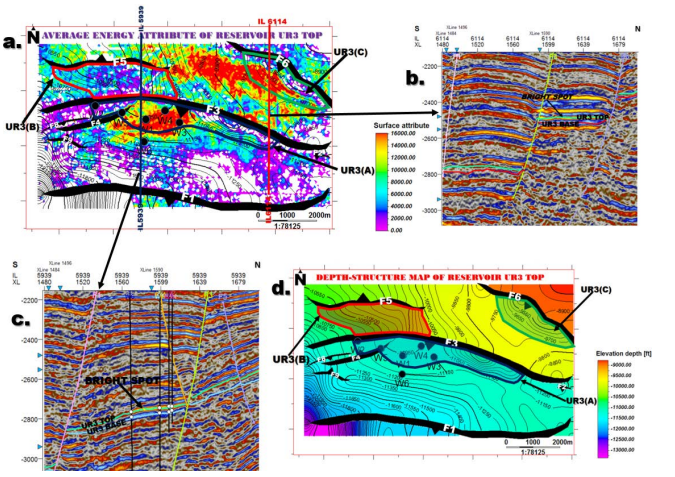


**Figure 15:** (a) average energy attribute of reservoir UR3 top showing the proven reserve (UR3(A)), the newly identified prospects (UR3(B) and UR3C)) and the highlighted high amplitude due to hydrocarbon effect. (b) Interpreted inline (IL 5939), showing the bright spot and reservoir UR3 top, which corresponds to the bright spot at the proven reserve area and (c) Interpreted inline section 6114 showing reservoir UR3 top and the anomalously high amplitude corresponding to prospect UR3(c). (d) The already proven reserve, which has been drilled by wells (W1 to 5) and the newly identified prospect areas, were delineated based on seismic attribute on fault and contour closure on a subtle rollover anticlinal structure at the hanging wall side of F3, F5 and F6, respectively.

**Reservoir petro physical models:** 3-D grids were constructed for the three identified reservoirs from where the petro physical results of the reservoirs were then upscale to assign the average values which were then used to populate each grid cell. After assigning each property to each grid cell at the well locations, the next thing was to distribute these properties in between well locations using a deterministic approach (Sequential Gaussian simulation algorithm) in order to preserve the multiplicity of the reservoirs. The models which are presented in Figures 16-21, show a fair to good distribution of the petro physical properties in the prospect areas. The three reservoirs are composed mainly of fine to coarse grained sands with minor shale intercalations as shown in the model. The total and effective porosities of reservoirs ranges from 19 to 35% and 18 to 30%, respectively with average total porosity of 25, 26 and 22% for reservoir UR1, UR2 and UR3, respectively and average effective porosity of 21, 22 and 20% for the three reservoirs, respectively. This trend indicates good to very good reservoir quality which is usually associated with well sorted medium to coarse grained sandstone. The averages of permeability across the three reservoirs are 1264, 1443 and 2180 mD while the shale volume, which also contribute to the total porosity, are 12, 14 and 15%. Water saturation is quite minimal with averages of 42, 43 and 37% in the three reservoirs with relatively high hydrocarbon saturation with averages of 58, 56 and 63%.

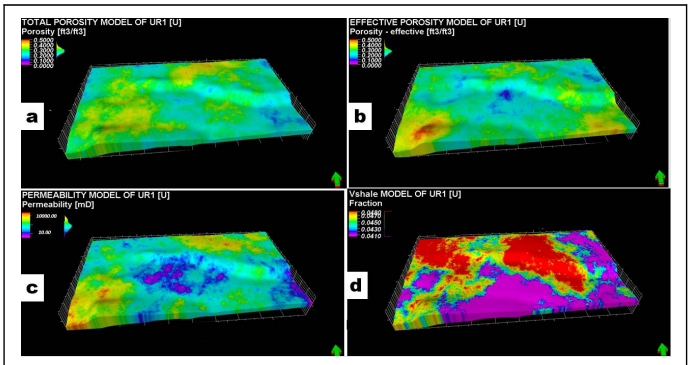


**Figure 16:** (a) Total and (b) effective porosities (c) permeability and (d) volume of shale models of reservoir UR1.

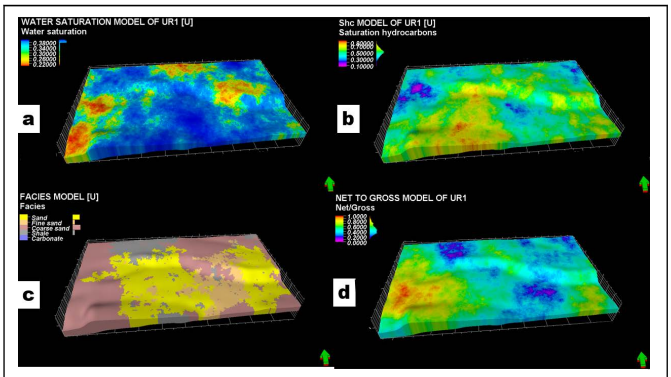


**Figure 17:** (a) Water and (b) hydrocarbon saturation (c) facies and (d) net-to-gross models of reservoir UR1.

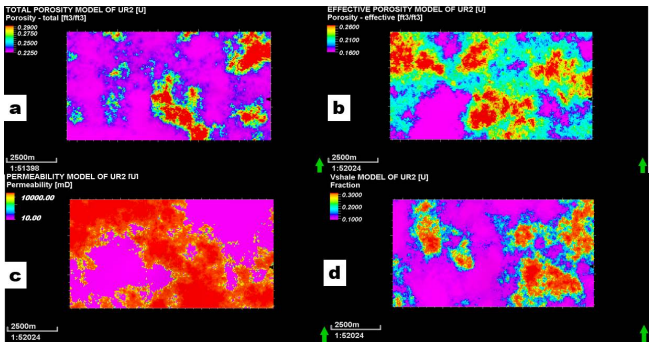


**Figure 18:** (a) Total and (b) effective porosities (c) permeability and (d) volume of shale models of reservoir UR2.

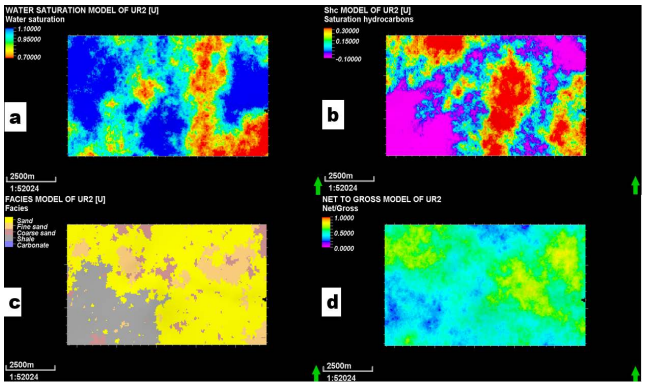


**Figure 19:** (a) Water and (b) hydrocarbon saturation (c) facies and (d) net-to-gross models of reservoir UR2.

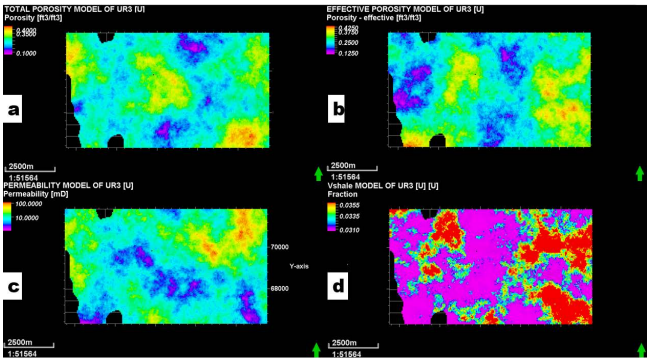


**Figure 20:** (a) Total and (b) effective porosities (c) permeability and (d) volume of shale models of reservoir UR3.

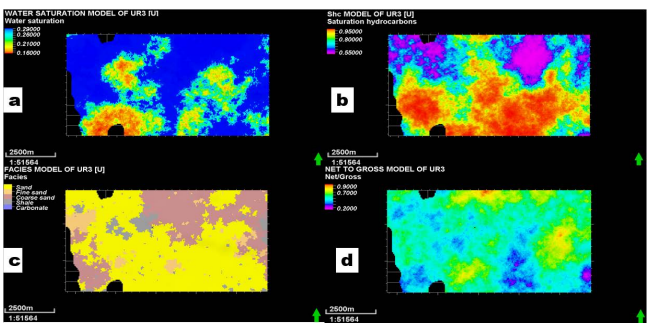


**Figure 21:** (a) Water and (b) hydrocarbon saturation (c) facies and (d) net-to-gross models of reservoir UR3.

**Volumetrics:** The deterministic and probabilistic approaches were used to calculate the Stock Tank Oil Initially in Place (STOIIP) for the three proven reserves and the four newly identified prospect areas. For the deterministic approach, the standard equation was used while the Monte Carlo simulation method was used for the probabilistic approach where the minimum, maximum and mean values of the proven reserve and prospect areas were used to generate the percentile of P0 to P10. However, the P10, P50 and P90 were chosen to represent the maximum, median and minimum values, respectively. The result of the both approaches and Figures 22 and 23, for better visualization. This result mainly depends on the reservoir thickness and enclosed area of the prospects; large thickness and enclosed areas result in large volumes and vice versa. UR1(A) contains gas cap, inferred from the anomalously high amplitude and a clear GOC could be seen. However, whereas other prospects also show anomalously high amplitude that may be attributed to gas presence, there is no clear GOC, both on the map and the wireline logs [11,12].

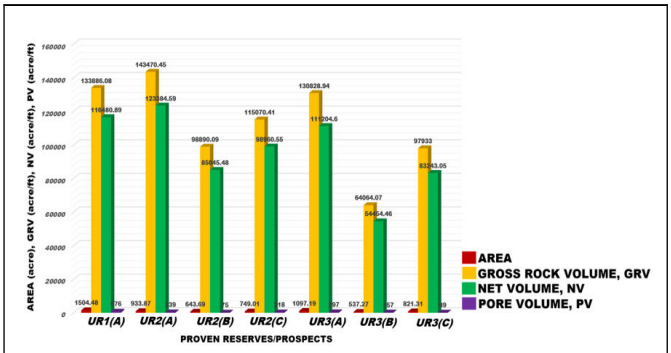


**Figure 22:** Bar chart showing the area, gross rock, net and pore volumes of the identified prospects and proven reserves.

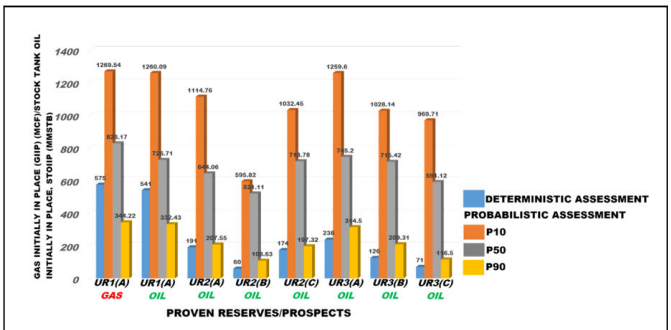


**Figure 23:** Bar chart showing the deterministic and probabilistic assessment of STOIIP, for the identified prospects and proven reserves (UR1(A)-UR3(C)).

## CONCLUSION

Integrating seismic, well log and other geological data is the key to making innovative hydrocarbon discoveries. By leveraging this approach, more sustainable and efficient energy industry can be built. However, this success largely depends on the data quality and the interpreter's skills and ability to identify subtle anomalies that may be attributed to hydrocarbon accumulations.

The combination of seismic amplitude analysis and realistic geological and petro physical models cannot be overemphasized. Reservoir static models were generated which helped to show the distribution fluid and petro physical properties such as porosity, permeability, water saturation and net to gross ratios. These models provided an insight on the distribution and volume of hydrocarbon in "USOR" field, thereby serving as a means of discovering, evaluating the reservoir and production potential of the prospects in the field. However, despite the effectiveness of these reservoir static models and the use of seismic volume attributes, such as utilized here, there is always a high risk of uncertainty associated with exploitation of hydrocarbon. It is therefore recommended that another form of seismic attribute analysis such as AVO should be carried out and core data should be made available and incorporated in the interpretation process.

## REFERENCES

1. Evamy BD, Haremboure J, Kamerling P, Knaap WA, Molloy FA, Rowlands PH. Hydrocarbon habitat of Tertiary Niger delta. AAPG Bull. 1978;62(1):1-39.
2. Tuttle ML, Charpentier RR, Brownfield ME. The Niger Delta petroleum system; Niger Delta Province, Nigeria, Cameroon and equatorial Guinea, Africa. US Geological Survey; 1999.
3. Bukola AB, Ibeneme SI, Osizemete AG, Obioha YE, Abba AU. Quality assessment and reserve estimation of the Egnaeja iron ore deposit, north-central Nigeria using integrated approach. Int J Earth Sci Geophys. 2020;6:037.
4. Rogers SJ, Fang JH, Karr CL, Stanley DA. Determination of lithology from well logs using a neural network. AAPG Bull. 1992;76(5):731-739.
5. Cvetkovic M, Velic J. Lithology prediction by artificial neural networks and preparation of input data on upper miocene sediments. Theory Appl Geomath. 2013;9-14.
6. Lopes DM, Andrade AJ. Lithology identification on well logs by fuzzy inference. J Petrol Sci Eng. 2019;180:357-368.
7. Sun Z, Jiang B, Li X, Li J, Xiao K. A data-driven approach for lithology identification based on parameter-optimized ensemble learning. Energy. 2020;13(15):1–15.
8. Sun J, Chen M, Li Q, Ren L, Dou M, Zhang J. A new method for predicting formation lithology while drilling at horizontal well bit. J Petrol Sci Eng. 2021;196:107955.
9. Xie Y, Zhu C, Hu R, Zhu Z. A coarse-to-fine approach for intelligent logging lithology identification with extremely randomized trees. Math Geosci. 2021;53(5):859-876.
10. Liu Z, Cao J, You J, Chen S, Lu Y, Zhou P. A lithological sequence classification method with well log *via* SVM-assisted bi-directional GRU-CRF neural network. J Pet Sci Eng. 2021;205:108913.
11. Hossain TM, Watada J, Aziz IA, Hermana M, Meraj ST, Sakai H. Lithology prediction using well logs: A granular computing approach. Int J Innov Comput Inf Control. 2021;17(1):225-244.
12. Zeng X, Xiao Y, Ji X, Wang G. Mineral identification based on deep learning that combines image and mohs hardness. Minerals. 2021;11(5):1–9.